A Graphical Method Predicting the Compressive Strength of Toughened Unidirectional Composite Laminates

Aidah Jumahat · Constantinos Soutis · Alma Hodzic

Abstract The in-plane shear and compressive properties of unidirectional (UD) HTS40/ 977-2 carbon fibre-toughened resin (CF/TR) laminates are investigated. Scanning Electron microscopy (SEM) and optical microscopy are used to reveal the failure mechanisms developed during compression. It is found that damage initiates by fibre microbuckling (a fibre instability failure mode) which then is followed by yielding of the matrix to form a fibre kink band zone that leads to final fracture. Analytical models are briefly reviewed and a graphical method, based on the shear response of the composite system, is described in order to estimate the UD compressive strength. Predictions for the HTS40/977-2 system are compared to experimental measurements and to data of five other unidirectional carbon fibre reinforced polymer (CFRP) composites that are currently used in aerospace and other structural applications. It is shown that the estimated values are in a good agreement with the measured results.

Keywords Polymer-matrix composites · Analytical modelling · Compressive strength · Fibre microbuckling · Toughened resins

1 Introduction

Carbon fibre reinforced polymer (CFRP) composites are well known high performance materials commercially used in the fabrication of aircraft structures [1]. Epoxy resins are the most versatile materials that are used as matrix in CFRP composites. Cured epoxy systems have properties such as excellent chemical and heat resistance, high adhesive strength and low shrinkage. However, they can exhibit brittle behaviour, which gives rise to poor fracture toughness, poor resistance to crack propagation and low impact strength, hence limiting their application as high performance materials in fields requiring high damage resistance and damage tolerance [2–5].

A. Jumahat · C. Soutis (✉) · A. Hodzic
Department of Mechanical Engineering, Aerospace Engineering, University of Sheffield,
Mappin street S1 3JD Sheffield, UK
e-mail: c.soutis@sheffield.ac.uk

The brittleness of cured epoxy resins is usually related to their highly cross-linked structure and low fracture energy or low effective energy absorption during fracture process. Therefore, most of the research developed in the past few decades focused on reducing the cross-linked density of the epoxy network or improving the relatively poor fracture properties by modifying commercially available epoxy resins with secondary components commonly called toughening agents. The development of thermosetting resins mixed with a toughening agent, such as thermoplastic, hydroxyl-containing thermoplastic oligomer, reactive flexibiliser, rubber, siloxane oligomers, elastomer, inorganic fillers or combinations of these, offers improved resin properties as have been reported by numerous researchers [2–9].

The compressive strength of CFRP UD laminates is primarily influenced by the shear yield stress τ_y and the initial fibre waviness (or misalignment) angle ϕ_0. Since fibre waviness can not be avoided during the manufacturing processes (due to mismatch of fibre/resin thermal properties), in recent advanced composite systems attention is devoted to the development of a tougher resin to increase the shear yield strength of the composite and extend the plastic hardening behaviour after shear yield. In theory, a toughened resin provides a good load transfer and lateral support to the fibres and gives better resistance to plastic deformation, and therefore improves the overall matrix-dominated properties such as in-plane shear and interlaminar shear strengths. However, many factors affect the toughness and capability of the toughened resin to support the fibres, such as the properties of the toughening agent, the curing conditions, dispersion and adhesion between the modifier and the epoxy matrix. Improper selection of the toughening agent and manufacturing method leads to a significant reduction to the overall compressive properties of the UD laminated composite.

This study investigates the physical and mechanical properties of UD HTS40/977-2 carbon fibre-thermoplastic toughened epoxy composite laminates. The fibre and resin volume fractions in the laminates and density, in-plane shear strength and modulus, compressive strength and modulus are measured according to ASTM standards D3410, D3039 and D3518 and CRAG test methods [10]. Damage initiation and propagation during uniaxial compressive loading are carefully monitored using strain gauges and examined by optical and scanning electron microscopy. A brief review of relevant fibre microbuckling models is presented together with an empirical formula for the composite shear response, expressed in terms of fibre and matrix material properties, that is developed to estimate graphically the UD compressive strength of the laminate. The predicted compressive strength of the UD HTS40/977-2 laminate is then compared to measured values and strength data of five other currently used CF/TR systems; results are summarized in Table 1.

2 Experimental Details

2.1 Materials and Fabrication Methods

The specimens were fabricated from carbon fibre/epoxy pre-impregnated tapes of 0.27 mm thickness and 300 mm tow width. The prepreg tapes were made of UD continuous high tensile strength carbon fibres (Toho Tenax HTS40 12 K 800tex) pre-impregnated with Cycom®977-2 toughened epoxy resin. The 977-2 matrix composed of epoxies and a proprietary polyaromatic thermoplastic resin. Incorporation of polyaromatic thermoplastic polymer into thermosetting resins offers significantly increased fracture toughness, without

Table 1 Summary of the analysed material systems

Fibre/Matrix	Type of matrix resin
HTS40/977-2[a]	Two-phase thermoplastic toughened epoxy
IM7/977-2[b,c]	Two-phase thermoplastic toughened epoxy
IM7/F655 [b,d]	Two-phase toughened bismaleimide (BMI) resin
T800/F3900 [b]	Incorporates micronsized elastomeric particles into the epoxy matrix to form a compliant interleaf between fibre plies after curing.
IM7/8551-7 [b,d]	Incorporates micronsized elastomeric particles into the epoxy matrix to form a compliant interleaf between fibre plies after curing.
IM6/1808I [b,e]	Incorporates a thin (25.4 μm) thermoplastic film applied to one side of the prepreg tape

[a] [current work], [b] [2–4], [c] [technical data sheet provided by Cytec Engineered Materials Ltd., available online: www.cytec.com], [d] [technical data sheet provided by Hexcel Corporation, available online: www.hexcel.com], [e] [30].

reduction in modulus, compared to unmodified epoxy as reported in [11–15]. The HTS40/977-2 pre-preg tapes are commercially available and supplied by Cytec Engineered Materials Ltd.

The pre-impregnated HTS40/977-2 tapes were fabricated using a hand lay-up process to produce an eight-ply UD panel and an eight-ply $[\pm45°]_{2s}$ laminate. The laminates were cured in a hot press at 177°C for 3 h in accordance to standard curing cycle recommended by the manufacturer. The $[0]_8$ and $[\pm45]_{2s}$ testing specimens for compression test and in-plane shear test, respectively, were prepared according to CRAG test method [10] and ASTM standards D3410, D3039 and D3518 as shown in Fig. 1. A short gauge-length specimen of 10 to 12 mm was used to evaluate the UD material compressive properties. The specimen dimensions are illustrated in Fig. 1a. Strain gauges of 120Ω were attached on both faces of five specimens to be tested in order to monitor the degree of Euler bending and measure axial strain and, hence, axial modulus. The test was considered invalid if there was a big difference in strain readings from the gauges on both faces of the specimen, which indicated that the specimen had undergone out-of-plane bending. In addition, a pair of longitudinal and transverse strain gauges was used to measure the Poisson's ratio of the UD laminate.

A specimen of 100 mm gauge length was used to evaluate in-plane shear properties of the HTS40/977-2 material. The specimen dimensions are presented in Fig. 1b. A pair of longitudinal and transverse strain gauges was used to measure the applied and transverse normal strain. The in-plane shear stress in the material coordinate system was directly calculated from the applied axial load whilst the related shear strain was determined from the longitudinal and transverse normal strain data collected by the strain gauges.

2.2 Characterisation Methods

Density of the HTS40/977-2 composite was measured using Density balance based on the Archimedes principle in distilled water. The measurement and calculation of CFRP density was conducted and calculated in accordance to ASTM standard D792. Fibre volume fractions of the UD and off-axis laminates were measured using an Image analyser technique. This technique requires the use of metallographic specimen preparation equipment, a reflected light microscope with a magnification of at least 400x, which has the capability of porting the image to a digital camera, a computer with image acquisition
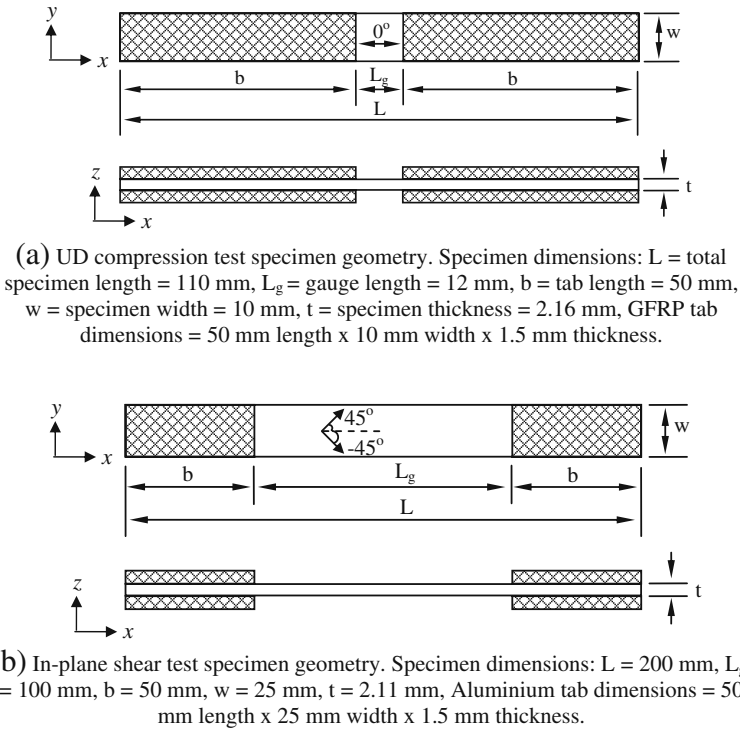
(a) UD compression test specimen geometry. Specimen dimensions: L = total specimen length = 110 mm, L_g = gauge length = 12 mm, b = tab length = 50 mm, w = specimen width = 10 mm, t = specimen thickness = 2.16 mm, GFRP tab dimensions = 50 mm length x 10 mm width x 1.5 mm thickness.

(b) In-plane shear test specimen geometry. Specimen dimensions: L = 200 mm, L_g = 100 mm, b = 50 mm, w = 25 mm, t = 2.11 mm, Aluminium tab dimensions = 50 mm length x 25 mm width x 1.5 mm thickness.

Fig. 1 $[0]_8$ and $[\pm45]_{2s}$ specimen geometry for **a** compression and **b** in-plane shear tests

card and image analysis software. A small section of laminate was prepared using standard metallographic techniques. The greyscale image was converted into a binary image where the pixels with values greater than the threshold value would be black and the pixels with values less than the threshold value would be white as shown in Fig. 2. The KSRUN version 3.0 ZEISS software automatically measured the fibre volume percentage based on the proportion of total field area to the total frame area.
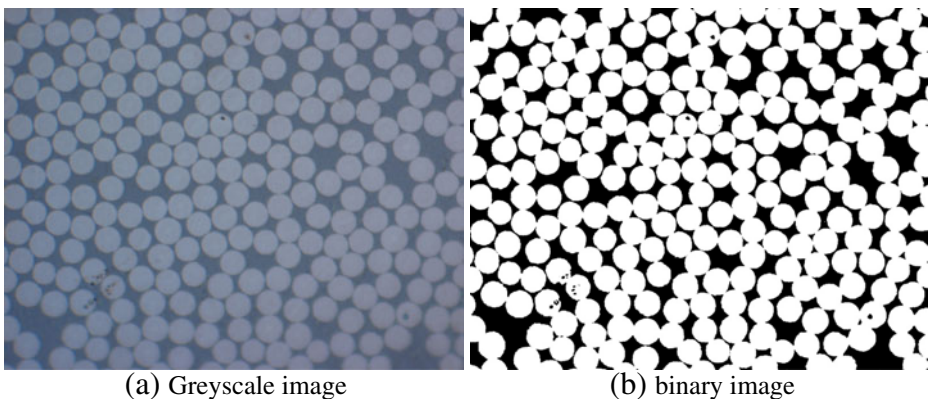

(a) Greyscale image   (b) binary image

Fig. 2 Typical greyscale and binary fibre images of HTS40/977-2 UD laminate at magnification of 1000x; fibre diameter is approximately 7 μm

Thermo-gravimetric analysis (TGA) was performed using a Perkin Elmer thermal analyzer to measure the fibre and resin volume fractions hence confirm the measured values by the image analyzer technique. TGA was also used to identify the rapid decomposition temperature of the constituent and to monitor the rate of degradation at specified temperature. The test was conducted according to ASTM Standard E1131. The isothermal temperature of 550°C [16] was applied. The selection of TGA heating programme is discussed in detail in section 3.1. The TGA curve plots showed the percentage weight change against the material's decomposition temperature. Data was collected using the TGA PYRIS software.

2.3 Compression Test and Damage Evaluation

The compression test was conducted in accordance to CRAG test method [10] and ASTM Standard D3410. A 250 kN servo-hydraulic machine with the Imperial College London (ICL) test fixture design [17, 18], as shown in Fig. 3a, was used to determine the compressive behaviour of the UD laminate. In this study, the compression on the UD specimens was performed at a constant compression rate of 1 mm/min. The specimen was tabbed at both ends and loaded in uniaxial compression. The ICL test fixture and specimen geometry were designed to generate a uniform one-dimensional stress state in the sample. All mechanical data, such as applied load, displacement, back-to-back longitudinal strains and transverse strain were recorded by a PC via a data acquisition system.

Several tests were stopped before the final failure occurred in order to examine the initial failure mode. The fractured specimen was prepared using the standard metallographic technique to be observed under the optical microscope at 50× to 1,000× magnification. The post-failure surfaces of the compression specimens were also observed using a Scanning Electron Microscopy (SEM) to identify the failure mechanisms involved during compression. The fractured specimen was attached to an aluminium plate using a carbon adhesive patch and then coated with a thin layer of gold at 20 mA and 0.05 torr pressure

(a) Compression test set-up   (b) In-plane shear test set-up
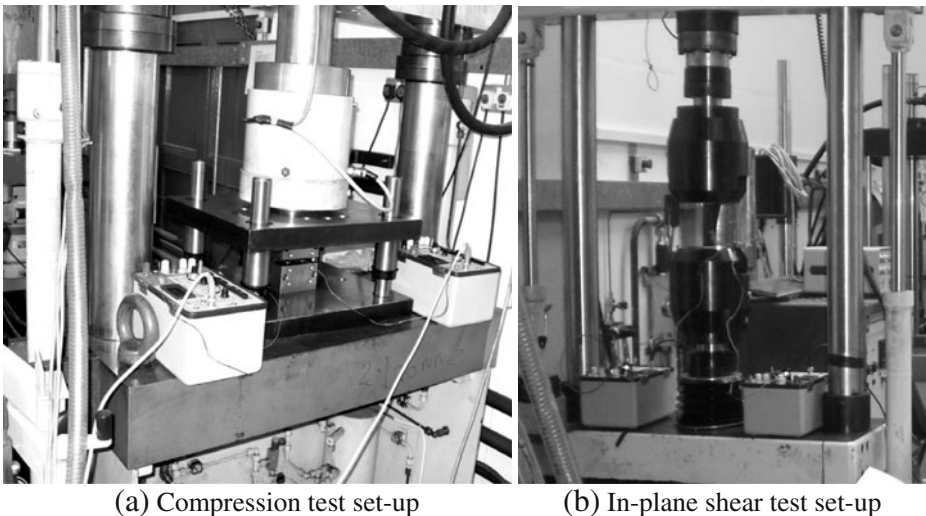
Fig. 3 Testing machines and fixtures assembly **a** 250 kN compression servo-hydraulic machine with ICL test fixture, and **b** Mayes 100 kN dynamic fatigue load frame and tensile test fixtures

using a Sputter Coater Unit EMSCOPE SC500 A. The specimen was then placed into the vacuum chamber of a scanning electron microscope at 10 kV and resolution 5 and ready to be viewed and examined.

The compressive behaviour of the HTS40/977-2 material is compared to data published in literature for other currently employed UD systems, and summarized in Table 1.

2.4 In-Plane Shear Test

The in-plane shear test was a uniaxial tension test of a ±45° laminate, which was performed in accordance to CRAG [10] and ASTM Standards D3518 and D3039. Figure 3b shows the Mayes 100kN dynamic fatigue load frame with the tensile test fixtures which is used to determine the tensile properties of the $[\pm45°]_{2s}$ laminate. Specimen was carefully aligned in the hydraulic grips of the test machine to avoid induced specimen bending. The tensile load was increased uniformly, at a 5 mm/min testing speed rate, to cause failure within 30–60 s. The data were collected using a data acquisition system.

3 Experimental Results of UD HTS40/977-2 Composite Systems

3.1 Physical Properties

Figure 4a shows the heating programme for TGA which consists of heating the specimen from room temperature to 550°C at a 10°C min^{-1} heating rate in nitrogen at 50 ml/min. The
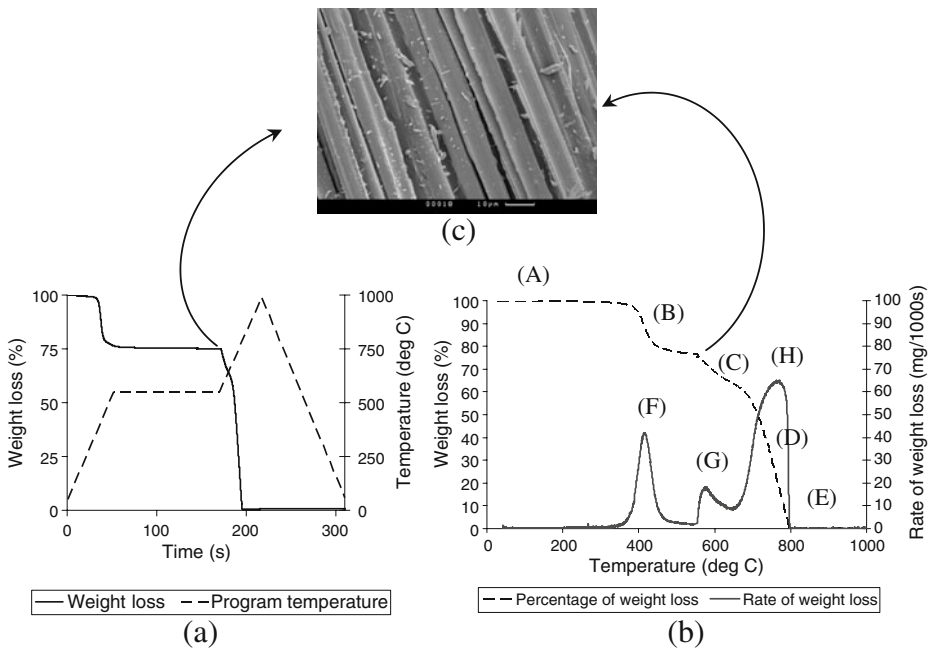

Fig. 4 Typical TGA results illustrating thermal effects on a HTS40/977-2 UD laminate; **a** Programme temperature of the specimen and weight loss as a function of sample temperature, **b** Percentage of weight loss and Rate of weight loss as a function of sample temperature, and **c** SEM micrograph of the specimen after isothermal temperature of 550°C

temperature was then kept at 550°C for 2 h to decompose the epoxy resin. The N_2 gas supply was then switched to air supply and the temperature was increased to 1000°C to decompose the remaining resin and graphite fibres. The residue (char) after isothermal temperature 550°C was collected for SEM observation. Figure 4b shows the percentage of weight loss and rate of weight loss as a function of sample temperature. The TGA profile illustrates five decomposition mechanisms as shown in Fig. 4b. Stage (A) the initial weight loss of about 0.3 wt.% occurred due to solvent or water vaporization. Stage (B) decomposition of epoxy resin of about 22 wt.%. The SEM observation on the char, as shown in Fig. 4c, confirmed the presence of remaining thermoplastic toughened epoxy resin which was deposited on the surface of the carbon fibre. Stage (C) decomposition of remaining resin of about 15 wt.%. Stage (D) decomposition of HTS40 carbon fibre of about 63 wt.% by oxidation at a maximum degradation temperature of 770°C (point H). Stage (E) the remaining residue is virtually 0%. This showed that there was no contamination in the CFRP composites. Figure 4b shows that the highest rate of degradation of the epoxy resin in nitrogen is at 418°C (point F) and the highest rate of degradation of the remaining thermoplastic toughened epoxy resin in air is 582°C (point G). A similar TGA results were reported in [19] for the degradation of the polyaromatic thermoplastic resin based on polyethersulphone.

The average diameter of the carbon fibre, which was measured using SEM and optical microscopic techniques, was 6.96 μm. The average density of the UD HTS40/977-2 composite laminate measured using the Archimedes principle in distilled water, was 1.54 g/cm^3. The average density of the [±45°]$_{2s}$ laminate was 1.59 g/cm^3. The average fibre volume fractions of UD and [±45°]$_{2s}$ HTS40/977-2 laminates were about 58% and 59%, respectively. These were measured using an Image analyzer technique. The total weight loss percentage of the 977-2 resin was about 37 wt.% and 63 wt.% for the HTS40 carbon fibre, as measured using TGA. The densities of the 977-2 resin and HTS40 carbon fibre, as provided by the manufacturers, were 1.31 g/cm^3 and 1.76 g/cm^3, respectively. Therefore the volume fractions of the resin and fibre as calculated using ASTM Standard D3171-99 were about 43.5% and 55.2%, respectively, hence the void volume fraction was 1.3%. The fibre volume fraction measured using TGA was 4.8% lower than that measured using the image analyzer technique. In this study, the initial degradation temperature of HTS40 carbon fibre is difficult to identify using TGA due to a high thermal stability of the toughened matrix. Degradation of the carbon fibre occurred at approximately 600°C and a similar value has been reported elsewhere such as in [19]. Therefore the fibre volume fraction measured using the image analyser technique will be used for the analysis in section 4.

3.2 Compressive Properties and Failure Modes

The compressive stress-strain response of a selected tested specimen is shown in Fig. 5. The longitudinal strain on front and back faces of the specimen was initially the same, however as the compressive load was increased, the strains diverged indicating some bending of the specimen or material softening due to internal damage. The graph exhibited an initially straight portion with an elastic modulus of 112 GPa measured at 0.25% applied strain and followed by a continuously curved portion with a tangential modulus at failure of approximately 40% less than that of the linear part. The average failure strength was 1,396 MPa and the mean failure strain 15,260 με or approximately 1.53% strain and the principal Poisson's ratio, $\nu_{12}=0.3$.

In general, fracture occurred within the specimen gauge length, implying that the test was successful, Fig. 6. The fracture mechanisms of the composite system under
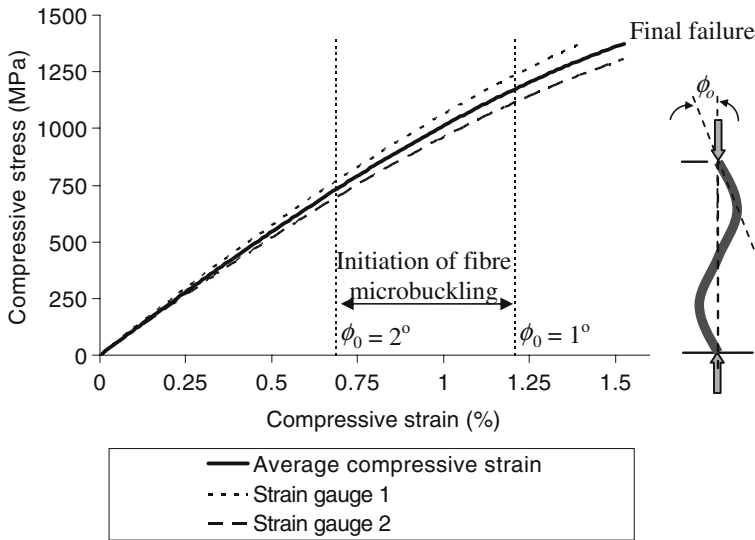
Fig. 5 A typical measured compressive stress-strain response of a UD HTS40/977-2 composite laminate. Triggering of fibre instability (microbuckling) depends on initial fibre waviness [20] and results to material softening

compression can be described in 2 stages; (1) fibre breakage in bending, accompanied by fibre/matrix debonding, called fibre microbuckling and (2) after microbuckling, two planes of fracture were formed, to create a narrow band inclined at an angle $\beta \approx 5°–25°$ to the horizontal axis called fibre kinking with a band width, w=60-100 μm (or $\approx$ 8 to 15 fibre diameters) as shown in Fig. 6. The fibre microbuckling failure mode and the subsequent kink band formation occurred without warning and immediately led to laminate breakage.
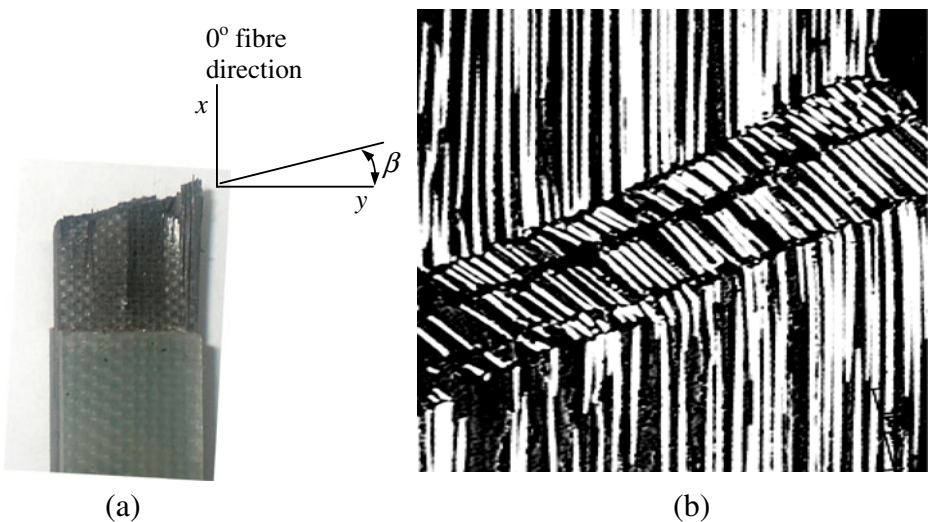

Fig. 6 Failure mode of a HTS40/977-2 UD specimen: **a** overall specimen failure (across width view); $\beta=$ 10° to 25° is called kink band inclination angle. **b** An optical microscopy image (at 200x magnification) of fibre kinking; kink band width (w) is 60 μm to 100 μm (or $\approx$ 8 to 15 fibre diameters)

SEM micrographs and optical micrographs of the failed specimens confirmed that failure of the UD HTS40/977-2 system was initiated by fibre microbuckling that was followed by yielding of the matrix to form fibre kinking (propagating across the specimen's width). Figure 7 shows SEM micrographs illustrating tensile and compressive surfaces on individual fibres that failed due to microbuckling. It is difficult to arrest and observe damage development in a unidirectional specimen since fracture occurs catastrophically with no previous warning. Specimen failure could initiate at the free edge or pre-existing material imperfections such as voids, fibre misalignments (waviness) and resin rich regions. In section 4.1, the Berbinau's fibre instability model [20] predicts initiation of fibre microbuckling at 735–1,173 MPa, for an assumed initial fibre misalignment of 2° or 1°, respectively. This falls within the material softening region observed in the macroscopic stress-strain curve shown in Fig. 5.

3.3 In-Plane Shear Properties

The in-plane shear stress-strain response obtained from a tensile test of a [±45]$_{2s}$ HTS40/977-2 composite laminate and a typical failed specimen is illustrated in Fig. 8. From the

(a)

(b)

The compressive surface appears to be irregular and serrated

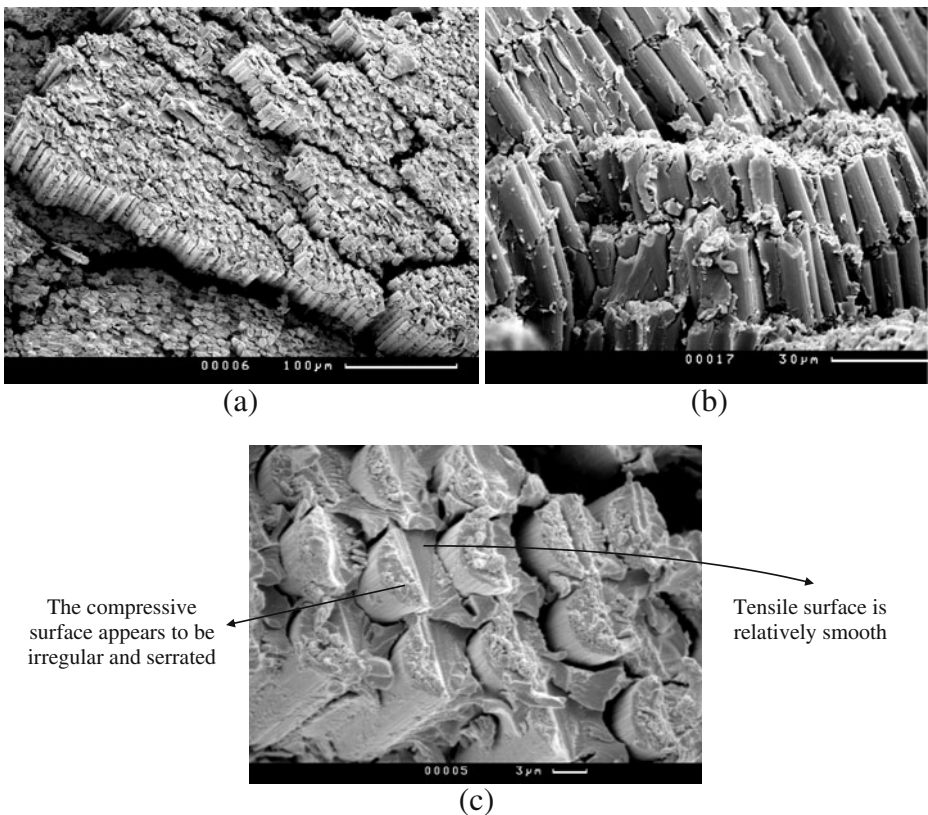Tensile surface is relatively smooth

(c)

Fig. 7 Fracture surface of a HTS40/977-2 UD specimen after compression; **a** SEM micrograph illustrates rows of buckled fibres and plastic deformation of the matrix, **b** SEM micrograph showing fibre microbuckling and fibre breakage, and **c** SEM micrograph illustrating tensile and compressive surfaces on an individual fibre failed due to bending (microbuckling)
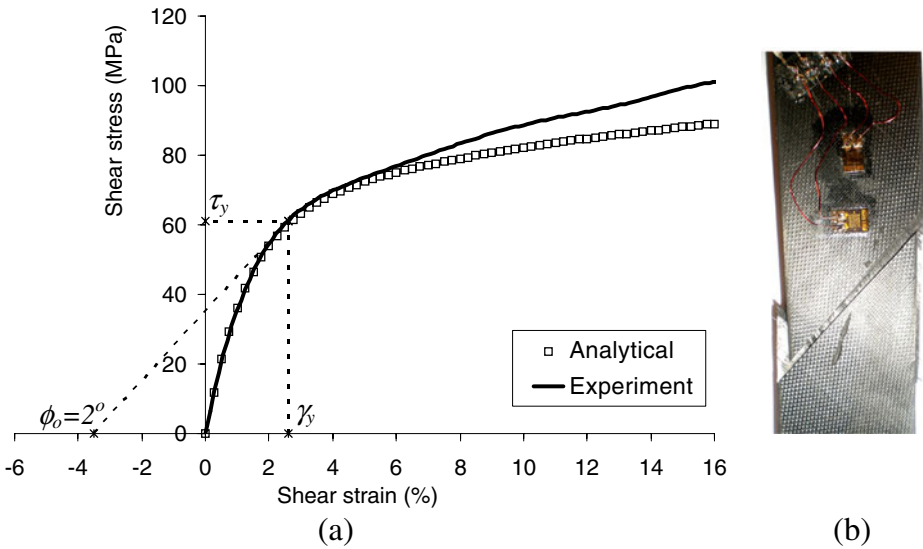
Fig. 8 **a** In-plane shear stress-strain response of a $[\pm45]_{2s}$ HTS40/977-2 composite laminate; a tangent to the curve, from a residual strain γ_0 that corresponds to an initial fibre waviness $\phi_0=2°$, is used to identify the yield point [27]. **b** Overall final failure

graph, the in-plane shear strength is 101 MPa at 16% maximum shear strain and the elastic shear modulus (tangent) measured at 0.25% applied shear strain is 4.8 GPa. After yielding, the shear modulus (secant) measured at γ_{ult} is reduced to 0.3 GPa. The yield point can be determined graphically, see Fig. 8. It is determined by drawing the tangent to the τ-γ curve from an initial shear strain $\gamma_0=3.5\%$ that corresponds to an initial fibre misalignment of about 2°. This is an average value measured using the Yurgartis method [21]. Figure 9a shows a typical micrograph taken from a $[0]_8$ HTS40/977-2 specimen which is sectioned at an angle of approximately $\theta_{cut}=5°$ to the 0°-fibre axis. The axial lengths of at least 400 fibres per sample, Fig. 9a, were measured and analysed automatically using an image
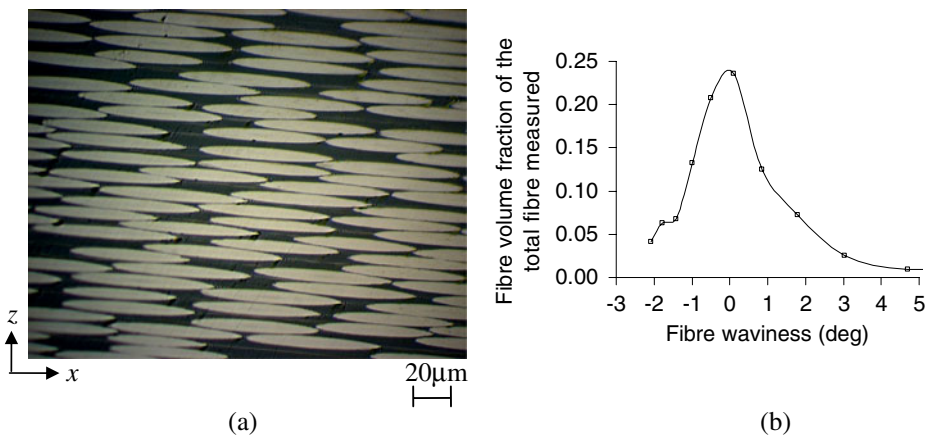

Fig. 9 **a** A typical optical micrograph taken from a $[0]_8$ HTS40/977-2 specimen sectioned at an angle of approximately 5° to the fibre axis and **b** Fibre angle distribution

analyser. The Yugartis technique [21] was applied to transform the angle of cut, θ_{cut}, into the fibre angle distribution for the initial fibre waviness ϕ_0 in the laminate as shown in Fig. 9b. From the graph, it is found that 91% of fibres lie within $\pm 1.8°$ of the 0°-fibre direction. The average fibre waviness was estimated as 2° with a standard deviation of 1.6. Assuming an initial fibre misalignment of 2°, the shear yield stress measured from the graph in Fig. 8a is found equal to 61 MPa at a shear yield strain $\gamma_y = 2.6\%$.

4 Prediction of UD Compressive Strength

The experimentally observed fracture mechanisms involved both fibre microbuckling and plastic fibre kinking. The microbukling of the fibre was governed by its initial waviness and the shear response of the matrix material. It is assumed that failure is triggered by fibre microbuckling from a region of misaligned fibres. The misaligned fibres break in two points upon reached maximum micro-bending deformation and two planes of fracture are created to form a fibre kink band; this scenario of failure events is based on extensive experimental observations. The kinked fibres disrupt the stability of the adjacent ones so that the neighbouring fibres also fail in buckling. A graphical method that uses the measured shear response of the composite and combines the fibre instability (microbuckling) and fibre kinking (post-buckling) modes observed in the experiments is described in the following section to predict the strength of UD HTS40/977-2 and other UD CF/TR composite systems reported in [2–4]; results are summarized in Tables 2–3. The physical and mechanical properties data obtained from the experimental work were incorporated in the prediction of compressive failure of various types of UD CF/TR composite laminates.

4.1 Prediction of the Compressive Strength of the HTS40/977-2 Composite System

The fibre instability mode or fibre microbuckling can be described by the Berbinau et al. [20] model that is based on an initial sinusoidal shape of misaligned fibres and accounts for the non-linear response of the matrix. Other factors, which affect the compressive failure strength of UD composite, such as fibre type, fibre diameter, fibre volume fraction and configuration of fibre waviness (wavelength and misalignment angle) were also considered in that model [20].

Table 2 Input data used for the compressive failure prediction of various UD CF/TR composite systems

Parameters	Input data					
	HTS40/ 977-2[a]	IM7/ 977-2[b]	IM7/ F655[b]	T800/ F3900[b]	IM7/ 8551-7[b]	IM6/ 1808I[b]
Fibre volume fraction, V_f	0.58	0.61	0.59	0.60	0.54	0.51
Fibre diameter, d_f (μm)	7.0	5.2	5.2	5.1	5.2	5.2
Fibre elastic modulus, E_f (GPa)	239	276	276	294	276	279
Laminate width, w (mm)	10	10	10	10	10	10
Laminate thickness, t_o (mm)	2.16	2.31	2.34	3.38	2.39	2.64
No. of plies, n	8	16	16	24	16	16
Ply thickness, t_p (μm)	270	144	146	141	149	165

[a] [current work], [b] [2–4]

Table 3 Stiffness and strength properties data of various types of UD CF/TR composite systems

Properties	Material data				
	IM7/977-2[a]	IM7/F655[a]	T800/F3900[a]	IM7/8551-7[a]	IM6/1808I[a]
Tensile Properties					
Longitudinal Elastic Modulus (GPa)	142 (165[b])	148 (161[c])	151	139 (159[c])	137 (128[d])
Longitudinal strength (MPa)	2537 (2690[b])	2518 (2730[c])	2415	2526 (2758[c])	1869 (1827[d])
Compressive Properties					
Longitudinal modulus (GPa)	141 (152[b])	146	146	130 (148[c])	134
Longitudinal strength (MPa)	908 (1580[b])	1076 (2167[c])	918	916 (1620[c])	802 (1276[d])
Failure strain (%)	0.69	0.80	0.66	0.72	0.66
Principal Poisson Ratio, ν_{12}	0.28	0.30	0.33	0.33	0.31
Shear Properties					
Elastic in-plane shear modulus, G_{12}^e (GPa)	4.8	5.6 (5.2[c])	5.1	4.5 (5.9[c])	4.0 (4.8[d])
In-plane shear strength, τ_{ult} (Mpa)	141	107 (125[c])	133	121 (117[c])	111 (127[d])

[a] [2–4], [b] [technical data sheet provided by Cytec Engineered Materials Ltd., available online: www.cytec.com], [c] [technical data sheet provided by Hexcel Corporation, available online: www.hexcel.com], [d] [30]

A general fibre microbuckling equation of a 0° fibre under compressive load was developed [20] by assuming that the fibre (possessing an initial misalignment) acted as an Euler slender column supported by a non-linear foundation (resin). Based on the fact that carbon fibres in the 0° UD laminates are not perfectly aligned with the loading direction (due to thermal mismatch), Berbinau et al. [20] modelled the initial fibre waviness by a sine function $v_0(x)$ as shown in Fig. 10a and derived the following 4th order differential equation that when solved gives the 0°-fibre stress as a function amplitude v:

$$E_f I_f \frac{d^4(v - v_0)}{dx^4} + \frac{A_f \sigma_{mb}}{V_f} \frac{d^2 v}{dx^2} - A_f G_{12}^{ep}(\gamma) \frac{d^2(v - v_0)}{dx^2} = 0 \qquad (1)$$

where E_f and I_f are the elasticity modulus and the second moment of area of the fibre, respectively. A_f is the fibre cross section area, V_f is the fibre volume fraction, $G_{12}^{ep}(\gamma)$ is the experimental nonlinear shear modulus as a function of shear strain, G_{12}^e and G_{12}^p are the elastic and plastic in-plane shear moduli, while τ_y and τ_{ult} are the yield and ultimate shear stress, respectively. The expression of $G_{12}^{ep}(\gamma)$ is given by:

$$G_{12}^{ep}(\gamma) = G_{12}^e \exp\left(-\frac{G_{12}^e \gamma}{\tau_y}\right) + G_{12}^p \exp\left(-\frac{G_{12}^p \gamma}{\tau_{ult} - \tau_y}\right) \qquad (2)$$

In this study, Eq. 1 was solved numerically using Fortran programming. This programme was compiled and executed via a commercial Fortran compiler to predict the compressive strength of UD HTS40/977-2 CFRP composite. The result was given by a relationship between the applied compressive stress σ^∞ and the maximum amplitude V of the buckled fibre during uniaxial compression. Failure of the axial fibre occurred when its amplitude V started to increase asymptotically. Table 2 summarizes the input data which are incorporated into the Fortran programme.
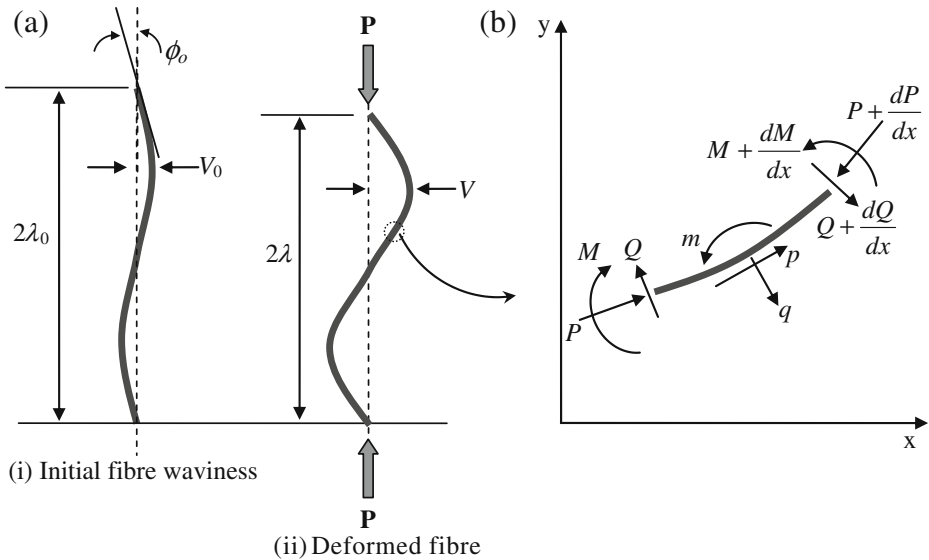
Fig. 10 **a** A schematic of fibre microbuckling mode [20] **b** Free body diagram for a fibre element [5]. $P=$ Axial compressive force, $Q=$Transverse shear, $M=$Bending moment, $p=$Applied distributed axial force, $q=$ Applied distributed transverse force, $m=$Applied distributed bending moment

Figure 11 presents the maximum amplitude V of the 0° buckled fibre versus the applied stress σ^∞ curves for the UD HTS40/977-2 CFRP composite laminate which are predicted using two different initial fibre misalignment angles; $\phi_o=1°$ and $\phi_o=2°$. The curves show that V increases slowly with increasing applied stress σ^∞ and then grows exponentially until
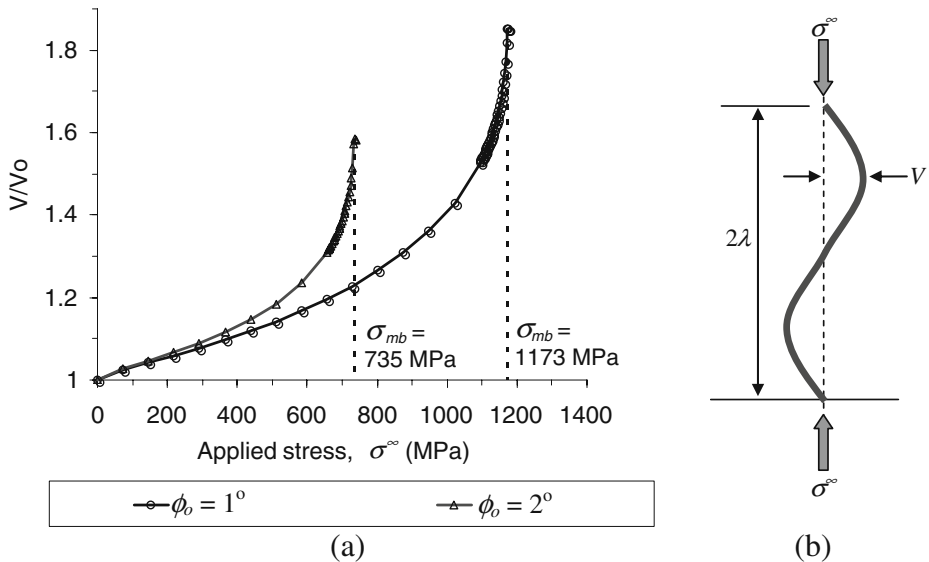

Fig. 11 **a** Fibre amplitude V normalised by initial fibre imperfection V_o versus applied compressive stress σ^∞. σ_{mb} is the critical stress at which fibre microbuckling is triggered and **b** schematic representation of a deformed fibre under axial compression

it reaches the maximum microbuckling stress σ_{mb} where the curve increases asymptotically. Fibre breakage is assumed to occur when the fibre amplitude increases without any significant changes in applied stress. The predicted microbuckling stress σ_{mb} of the HTS40/977-2 UD composite laminate at $\phi_o=1°$ is 1,173 MPa, which is 16% lower than the experimentally measured compressive strength. The microbuckling stress is reduced to 735 MPa at an assumed value $\phi_o=2°$. From the fibre waviness distribution as shown in Fig. 9b, most of the fibres lie in between $\pm2°$ from the 0° fibre axis. If the mean fibre waviness of $\phi_o=2°$ is applied, the compressive strength predicted using Berbinau's model is about 47% less than the measured value.

Berbinau's model [20] underestimates the actual compressive strength because the predicted value corresponds to the critical stress at which fibre instability or micro-buckling initiates and not necessarily the final failure stress of the whole laminate caused by both fibre microbuckling (damage initiation) and plastic kinking (damage propagation mechanism) as discussed earlier. In the fibre microbuckling analysis [20], the compressive strength of the composite is considered as the value at which fibre microbuckling is triggered suggesting catastrophic failure of the composite. However, in this tougher composite system examined here it is assumed that the buckled fibres continue to support load and final failure occurs when the fibre kink band zone has propagated across the specimen width. After fibre microbuckling, the compressive response is represented by plastic deformation of the composite that is called plastic fibre kinking failure mode.

In Fig. 12 a graphical method to predict the UD ultimate compressive strength is presented that is based on the composite's shear response. The measured shear response
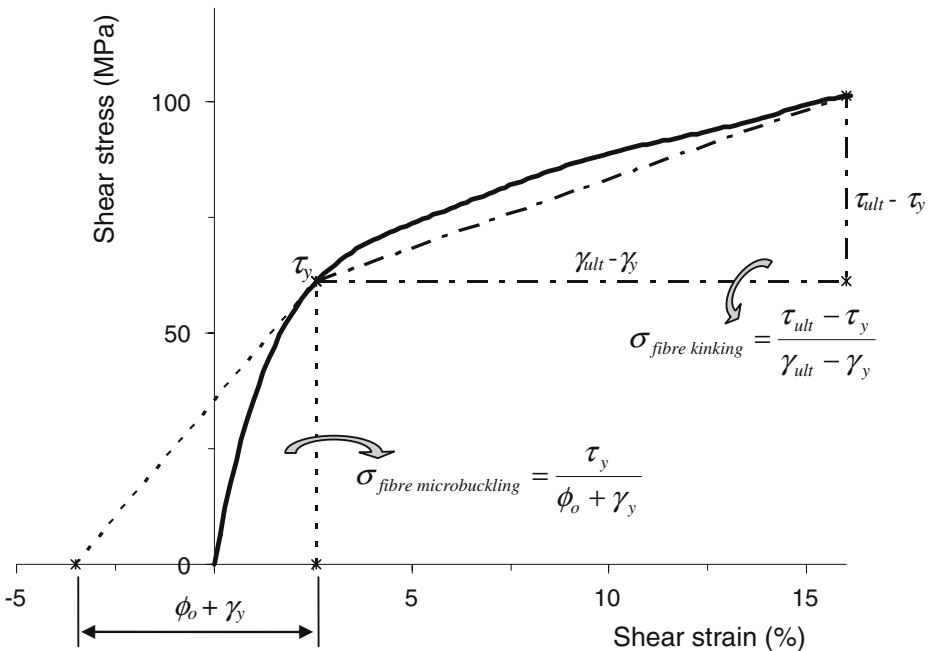

Fig. 12 A graphical representation of fibre microbuckling (elastic deformation) and fibre kinking (plastic deformation) stresses for a HTS40/977-2 UD laminate, determined from the shear stress- shear strain response

shown in Fig. 8a or alternatively an empirically derived expression, Eq. 3, that fits well the experimental curve can be used to estimate the strength:

$$\tau(\gamma) = \tau_y\left(1 - \exp\left(-\frac{G_{12}^e\gamma}{\tau_y}\right)\right) + \left(\tau_{ult} - \tau_y\right)\left(1 - \exp\left(-\frac{G_{12}^p\gamma}{\tau_{ult} - \tau_y}\right)\right) \quad (3)$$

It is assumed that the compressive strength of the UD composite is proportional to the summation of the tangent shear modulus (measured at γ_y), which corresponds to fibre microbuckling contribution, plus the secant shear modulus (measured at γ_{ult}) that represents the resistance to fibre kinking propagation. The first part of the expression for the UD compressive strength, Eq. 4a and 4b, resembles the fibre kinking model by Budiansky [22], but here the fibre microbuckling initiation ($\sigma_{m/buckling\ init}$) and fibre kinking propagation ($\sigma_{kinking\ propg}$) stress values are added to estimate the ultimate strength:

$$\sigma_c = \sigma_{m/buckling\ init} + \sigma_{kinking\ propg} \quad (4a)$$

or

$$\sigma_c = \frac{\tau_y}{\phi_0 + \gamma_y} + \frac{\tau_{ult} - \tau_y}{\gamma_{ult} - \gamma_y} \quad (4b)$$

In earlier work by Rosen [23], it was assumed that the compressive strength is proportional to the elastic shear modulus, $\sigma_c \approx G$, which of course over estimates the UD strength of the HTS40/977-2 composite laminate by more than three times. Budiansky's formula $\sigma_c = \frac{\tau_y}{\phi_0 + \gamma_y}$ for the HTS system would give a strength value of 1,000 MPa assuming $\phi_0 = 2°$, while the predicted compressive strength using the combined modes model, Eq. 4b, is about 1,300 MPa, which is 7% lower than the measured compressive strength, see Fig. 13. Further support of damage development described by Eq. 4b comes from observations made in multidirectional specimens with an open hole loaded in compression [24, 25] where the location of damage initiation is known and its propagation easier to monitor. In those studies failure initiates near the edge of the hole due to high localised stress [26] in the form of fibre microbuckling and propagates across the specimen width as fibre kinking, causing ultimate failure when the fibre kink band zone reaches a critical length of 2–3 mm, depending on laminate stacking sequence and hole size.

It can be said that the graphical method presented in Fig. 12 offers a convenient way of estimating the UD compressive strength provided that the initial fibre waviness and the $\tau-\gamma$ curve of the composite system are known; in addition the method captures the actual
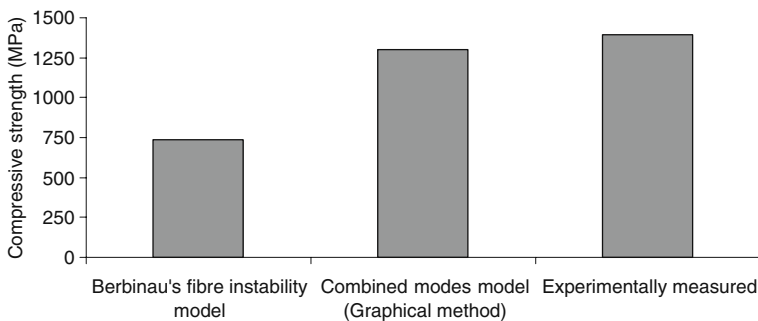

Fig. 13 Comparison of predicted and measured compressive strength of the UD HTS40/977-2 composite laminate. The critical stress for fibre instability is also shown

damage phenomena observed in this and previous experimental works [27, 28]. The empirical formula, Eq. 3, developed for the τ–γ shear response and expressed in terms of fibre and resin material properties appears to be very convenient to use in this graphical representation of the composite's compressive strength and the whole analysis can be easily implemented in a computer programme to perform a parametric study. The user could identify which and by how much each material variable (initial fibre waviness/ misalignment, shear modulus, shear yield stress/strain) affects the compressive strength of the UD laminate and select material appropriately.

4.2 Prediction of Compressive Strength of Various Types of CF/TR Systems Using the Graphical Method

The fibre microbuckling and plastic kinking failure modes have been observed to be the dominant compressive failure mechanisms in currently used carbon fibre/toughened epoxy composite systems. In CFRP composites, the identification of critical failure modes is not easily accomplished because fracture of composites is usually instantaneous and catastrophic. Moreover, the valid measurement of the compressive response of CFRP has always presented difficulties [28, 29]. For example, the experimentally measured compressive strength data presented in [2–4] and summarized in Table 3 were considered as non valid because of premature failures that resulted in relatively low UD compressive strengths. Most of the end-loaded test specimens failed early by longitudinal fibre/matrix splitting and exhibited premature failure characterised as end brooming or fibre crushing rather than fibre breakage [2]. The values for the stiffness properties were accepted since they were measured at 0.2% applied compressive strain and below the value at which axial splitting occurred. Here, the graphical modelling method discussed earlier, with appropriate input material parameters, was employed to predict the compressive strength of these UD CF/TR composite systems described in [2–4]; Table 1 summarises the material properties used. Table 2 presents the physical properties of the laminate, initial configuration of the fibre and the properties of the fibre used in these CFRP systems. The stiffness and strength data reported in [2–4, 30] are given in Table 3. An initial fibre misalignment of ϕ_o=2° and initial fibre half-wavelength λ_o=10d_f were assumed in the model for all composites since these are considered as typical values observed in both current work and elsewhere [5, 17, 19–22]. In addition, the shear stress-strain response of these composite systems was predicted using Eq. 3 by assuming ϕ_o=2°, shear yield strain γ_y=2.6% and shear strain at break γ_{ult}=16%.

Figure 14 presents the maximum amplitude V of the 0° buckled fibre versus the applied stress σ^∞ for the various types of CF/TR UD composite systems assuming ϕ_o=1° and ϕ_o=2°. Figure 14b shows the predicted value of microbuckling stress, using Eq. 1, for the IM6/1808I, IM7/8551-7 and IM7/977-2 UD composite systems. This is up to 54% lower than the ultimate strength data, see Table 3. When an initial fibre misalignment of 1° is used, the predicted critical stress is 12–29% lower than the measured ultimate value.

The predicted compressive strengths of the IM6/1808I, IM7/8551-7 and IM7/977-2 UD composite systems using the combined modes model, shows a good agreement with the measured values, as seen in Fig. 15 and Table 3. It should be noted that the predicted strength value is sensitive to the input data used in the model. The graphical model inaccurately predicted the strength of the toughened BMI resin composite system (IM7/ F655) due to lack of information regarding its non-linear shear stress-strain behaviour that is required in the analysis. The strength data provided by the manufacturer of this system is also in disagreement with the measured value reported in [2–4] maybe due to different
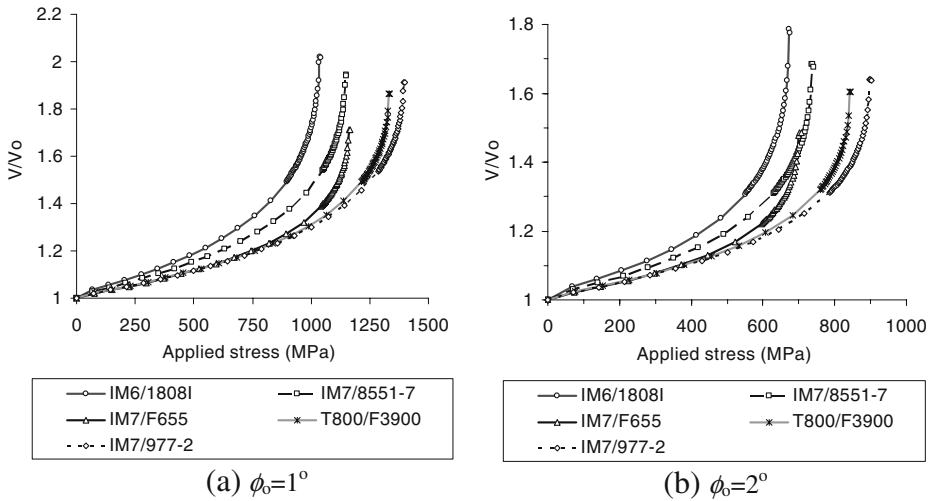
Fig. 14 Variation of 0° fibre amplitude with applied stress curves predicted using the fibre instability model [20], assuming **a** ϕ_o=1° and **b** ϕ_o= 2°, for five different types of UD CF/TR composite systems

experimental set up and resulted failure modes. Other more mathematically rigorous models that can be used to describe the compressive behaviour of UD composite laminates could be found in [31, 32].

The present analysis further confirmed that the compressive strength of a the UD CF/TR composite laminate was influenced by several factors such as in-plane shear properties, fibre properties, fibre volume fraction and configuration of fibre waviness as shown in Tables 2 and 3. The Berbinau et al. [20] fibre instability model is a good predictive tool for
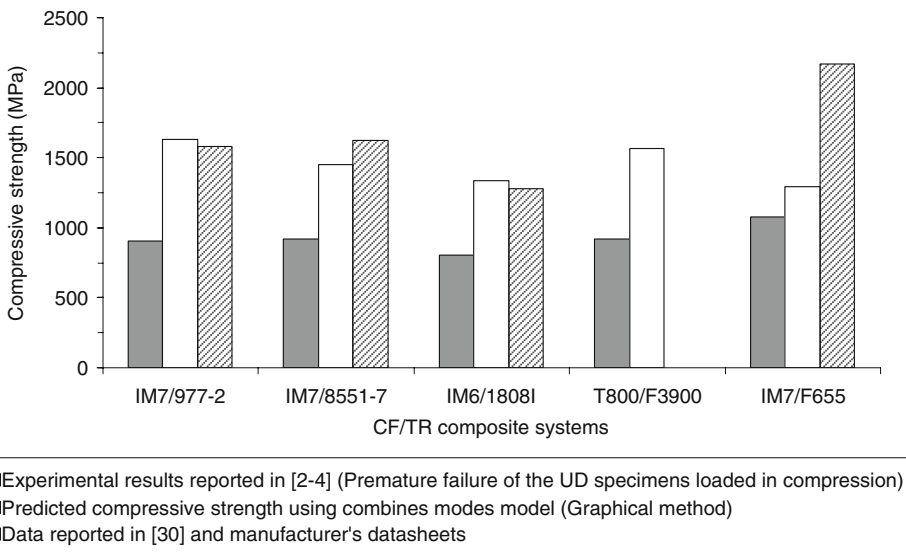

Fig. 15 Predicted compressive strength for several types of UD CF/TR composite systems using the graphical method compared to measured data presented in Table 3

microbuckling initiation but not necessarily for estimating the ultimate compressive strength, especially in carbon fibre/toughened epoxy systems where further load is required for laminate fracture. A real time non-destructive evaluation method [33, 34] could be very desirable to monitor damage initiation and propagation in compression but this is an area for further future work.

5 Conclusions

The failure of the HTS40/977-2 CF/TR UD composite, as observed from extensive optical and SEM work was initiated by fibre microbuckling, which is a fibre instability failure mode, followed by fibre kinking, which is a plastic deformation (post-buckling) phenomenon. The experimental observations led to the development of a graphical method (combined modes model) that is based on the shear response of the composite, to estimate the ultimate compressive strength of the HTS40/977-2 system. The procedure accounts for the load (stress) required to trigger fibre microbuckling and subsequent load required for fibre kinking propagation. This method mathematically resembles the Budiansky fibre kinking analysis that explains the significance of shear properties on the UD compressive behaviour and successfully predicted the compressive strength of the HTS40/977-2 system and other UD CF/TR composite systems that are currently used in aerospace and other structural applications.

References

1. Soutis, C.: Fibre reinforced composites in aircraft construction. Prog. Aerosp. Sci. **41**(2), 143–151 (2005)
2. Cano, R.J., Dow, M.B.: Properties of five toughened matrix composite materials. NASA technical paper 3254. National aeronautics and space administration (NASA) Langley research centre, USA (1992).
3. Smith, D.L., Dow, M.B.: Properties of three graphite/toughened resin composites. NASA technical paper 3102. NASA Langley research centre, USA (1991)
4. Dow, M.B., Smith, D.L.: Properties of two composite materials made of toughened epoxy resin and high strain graphite fibre. NASA technical paper 2826. NASA Langley research centre, USA (1988)
5. Hahn, H.T., Williams, J.G.: Compression failure mechanism in unidirectional composites. In: Whitney, J. M. (ed.) Composite materials: testing and design (seventh conference) ASTM STP 893, pp. 115–139. ASTM, Philadelphia (1986)
6. Janke, C.J., Dorsey, G.F., Havens, S.J., Lopata, V.J.: Toughened epoxy system and a method thereof. United States Patent 5726216. US patents, USA (1998)
7. Bagheri, R., Pearson, R.A.: Role of particle cavitation in rubber-toughened epoxies: II. Inter-particle distance. Polymer **41**, 269–276 (2000)
8. Lu, R., Plummer, C.J.G., Cantwell, W.J., Kausch, H.H.: Toughening mechanisms in modified epoxy resins with different crosslink densities. Polym. Bull. **37**, 399–406 (1996)
9. Pearson, R.A., Yee, A.F.: Toughening mechanisms in thermoplastic-modified epoxies: I. Modification using poly(phenylene oxide). Polymer **34**, 3658–3670 (1993)
10. Curtis, P.T.: CRAG test methods for the measurement of the engineering properties of fibre reinforced plastics. RAE Technical Report 85099. Royal Aircraft Establishment, Farnborough UK (1985)
11. Sabo, J., Strait, L.H., Strauch, E.C., Koudela, K.L., Giannetti, W.B.: Processing and characterization of thick laminated composites. In: Composites Materials, Mechanics and Processing, Proceedings of the American Society for composites, pp. 574–586. CRC Press, USA (1994)

12. Pethrick, R.A., Hollins, E.A., McEwan, I., MacKinnon, A.J., Hayward, D., Cannon, L.A., Jenkins, S.D., McGrail, P.T.: Dielectric, mechanical and structural, and water absorption properties of a Thermoplastic-modified epoxy resin: Poly(ether sulfone)−Amine cured epoxy resin. Macromolecules **29**(15), 5208–5214 (1996)
13. McGrail, P.T.: Polyaromatics. Polym. Int. **41**, 103–121 (1996)
14. Di Pasquale, G., Motta, O., Recca, A.: New high-performance thermoplastic toughened epoxy thermosets. Polymer **38**(17), 4345–4348 (1997)
15. Akay, M., Cracknell, J.G.: Epoxy resin-polyethersulphone blends. J. Appl. Polym. Sci. **52**(5), 663–688 (1994)
16. Moon, C.R., Bang, B.R., Choi, W.J., Kang, G.H., Park, S.Y.: A technique for determining fiber content in FRP by thermogravimetric analyzer. Polym. Test. **24**(3), 376–380 (2005)
17. Lee, J., Soutis, C.: A study on the compressive strength of thick carbon fibre–epoxy laminates. Compos. Sci. Technol. **67**, 2015–2026 (2007)
18. Lee, J.H.: Compressive behaviour of composite laminates before and after low velocity impact. PhD thesis. University of London (2003)
19. Cheremisinoff, N.P.: Advanced polymer processing operations. William Andrew, USA (1998)
20. Berbinau, P., Soutis, C., Guz, I.A.: Compressive failure of 0° unidirectional carbon-fibre-reinforced plastic (CFRP) laminates by fibre microbuckling. Compos. Sci. Technol. **59**, 1451–1455 (1999)
21. Yurgartis, S.W.: Measurement of small angle fiber misalignments in continuous fiber composites. Compos. Sci. Technol. **30**, 279–293 (1987)
22. Budiansky, B.: Micromechanics. Comput. Struct. **16**(1), 3–12 (1983)
23. Rosen, B.W.: Mechanics of composite strengthening. In: Fibre composite materials, Proceedings of the American Society for metals, pp. 574–586. American society for metals USA (1965)
24. Soutis, C., Curtis, P.T.: A method for predicting the fracture toughness of CFRP laminates failing by fibre microbuckling. Compos. A **31**(7), 733–740 (2000)
25. Soutis, C., Smith, F.C., Matthews, F.L.: Predicting the compressive engineering performance of carbon fibre-reinforced plastics. Compos. A **31**(6), 531–536 (2000)
26. Hu, F.Z., Soutis, C., Edge, E.C.: Interlaminar stresses in composite laminates with a circular hole. Compos. Struct. **37**(2), 223–232 (1997)
27. Soutis, C.: Compressive strength of unidirectional composites: measurement and prediction. ASTM-STP1242 **13,**168–176 (1997)
28. Jumahat, A., Soutis, C., Jones, F.R., Hodzic, A.: Fracture mechanisms and failure analysis of carbon fibre/toughened epoxy composites subjected to compressive loading. Compos. Struct. **92**(2), 295–305 (2010)
29. Soutis, C.: Compression testing of pultruded carbon fiber-epoxy cylindrical rods. J. Mater. Sci. **34**, 3441–3446 (2000)
30. Madan, R.C.: Composite transport wing technology development. NASA Contractor Report 178409. NASA Langley Research Centre USA (1988)
31. Guz, I.A., Soutis, C.: Predicting fracture of layered composites caused by internal instability. Compos. A **32**(9), 1243–1253 (2001)
32. Guz, I.A., Soutis, C.: Compressive fracture of non-linear composites undergoing large deformations. Int. J. Solids Struct. **38**(21), 3759–3770 (2001)
33. Diaz Valdes, S.H., Soutis, C.: Real-time non-destructive evaluation of fibre composite laminates using low-frequency Lamb waves. J. Accoust. Soc. America. **111**(5), 2026–2033 (2002)
34. Diamanti, K., Soutis, C., Hodgkinson, J.M.: Piezoelectric transducer arrangement for the inspection of large composite structures. Compos. A **38**(4), 1121–1130 (2007)